Int. J. Electrochem. Sci., 14 **(2019)** 11212 – 11224, doi: 10.20964/2019.12.29

International Journal of
ELECTROCHEMICAL
SCIENCE
www.electrochemsci.org

New Electrochemical Immunosensor of Au/Holey Graphene Oxide and Au/ZnO for Sensitive Detection of Carcinoembryonic Antigen

Aihua Jing[1], *Qiong Xu*[1], *Wenpo Feng*[1], *Yu Li*[1] *and Gaofeng Liang*[2,*]

[1] School of Medical Technology and Engineering, Henan University of Science and Technology, Luoyang 471003, P. R. China
[2] Medical college, Henan University of Science and Technology, Luoyang 471003, P. R. China
[*]E-mail: lgfeng990448@haust.edu.cn

Received: 1 August 2019 / *Accepted:* 19 September 2019 / *Published:* 29 October 2019

A sandwich-type electrochemical immunosensor was developed using Au/ZnO as a nonenzymatic label for the ultrasensitive detection of a tumour biomarker carcinoembryonic antigen (CEA). Au nanoparticle-decorated holey graphene oxide (Au/HGO) was synthesized according a simple hydrothermal procedure and modified on an electrode to have enhanced conductivity, large surfaces areas and good adsorption of immobilizing antibodies (Ab_1). Subsequently, horseradish-peroxidase (HRP)-functionalized Au/ZnO (Ab_2/HRP-Au/ZnO) was fabricated to label the secondary antibodies (Ab_2). The Ab_2/HRP-Au/ZnO catalysed the reduction of H_2O_2 in the sandwich-type immunoreactions. An enhanced sensitivity was obtained. Moreover, the proposed immunosensor showed a wide linear range from 0.001 ng/mL to 100 ng/mL with a detection limit of 0.6 pg/mL (S/N = 3) under the optimal experimental conditions. The disposable immunosensor has high sensitivity, long-term stability, and has clinical value in cancer screening and in appropriate point of care diagnostics.

Keywords: Au nanoparticle/holey graphene oxide; Au/ZnO; signal amplification; sandwich-type electrochemical immunosensor

1. INTRODUCTION

Malignant tumours are characterized by high morbidity and mortality and a serious dangers to human health [1, 2]. Carcinoembryonic antigen (CEA) is a reliable broad spectrum tumour marker that is one of the most efficient prognostic indicators of cancer in clinical diagnosis [3]. The sensitive detection of low levels of CEA in serum samples is decisive for early identification and clinical treatment of tumours[4]. To date, a number of sophisticated methods have been used to measure CEA, including immunohistochemistry (IHC) [5], real time PCR [6], microarray chips [7], fluorescence in

situ hybridization (FISH) [8], chromogenic [9], chemiluminescence immunoassay [10] and electrochemistry [11]. Among these strategies, the antibody-based biosensors [12], i.e., immunosensors, have certain distinct advantages, including high selectivity, short assay time, excellent sensitivity and low requirements of the amount of the analyte; the use of the biosensors have attracted considerable attention in the quantitative detection of a set of tumour markers, including CEA. Specifically, electrochemical sandwich-type immunosensors based on nanomaterials with perfect properties conjugated with detection antibodies (Ab_2) for signal amplification are outstanding methods characterized by high selectivity and excellent sensitivity. Nonetheless, ultratrace CEA detection has a room for critical improvements. Signal amplification of the immunosensors is based on the interface of the modified electrode. A high immobilizing efficiency of the biorecognition layer and a superior nanocarrier are of critical importance for increasing the sensitivity of an immunosensor. Therefore, specific nanomaterials are urgently needed.

Graphene, a single-atom-thickness carbon sheet, has attracted considerable attention due to multiple outstanding electronic, optical, and thermal properties[13]. Typically, graphene oxide with nanopore macrostructures is expected to exhibit improved surface areas and substantially higher electron transfer dynamics compared with those of non-holey graphene oxide [14]. The unique nanostructure and excellent conductivity make graphene a potential material for the fabrication of electrochemical immunosensors. Gold nanoparticles (Au NPs) have good electrical conductivity and excellent biocompatibility and have been used as the substrate material for the incubation of the capture antibody (Ab_1) in immunosensors [15]. Au NPs on the interface of an electrode can improve the speed of the electron transfer and provide a superior microenvironment for capturing additional antibody (Ab_1); therefore, Au NPs improve the sensitivity of the sensor. Thus, in this work, Au NP-decorated holey graphene oxide (HGO) was selected as the matrix material to assemble an immunosensor for the selective and reproducible electrochemical detection of cancer biomarker.

The quantitative assay of CEA by the designed immunosensor was able to determine whether the Ab_2 label can properly amplify the signal. The ZnO nanostructures have various technological applications as sensors in bio-medicine and in drug delivery; these nanostructures have a number of intrinsic advantages, including high catalytic efficiency, low toxicity, biocompatibility, biodegradability, unusual optical properties, etc. [16, 17]. However, ZnO electrochemical immunosensors may generally suffer from certain characteristics that prevent charge transfer due to the semiconductor nature of ZnO. Alternatively, hybrid metal/semiconductor composite matrices, such as gold-doped ZnO composites, have been utilized to increase the electron transport efficiency and to improve catalytic ability due to versatile properties of gold, such as its excellent electron transfer rate, strong adsorption of biological molecules, and enhanced electrochemical activity. For example, Zhao et.al. fabricated gold nanoparticle-modified zinc oxide nanorods (Au/ZnO) with enhanced electro-catalytic properties for the sensitive detection of L-lactate [18]. Wei and co-workers reported the hydrothermal synthesis of ZnO nanorods/Au hybrid nanocomposites with efficient electrocatalytic activities [19].

In this work, a novel sandwich-type electrochemical immunosensor was designed for the ultrasensitive detection of CEA. Scheme 1 displays the fabrication process of the sandwich-type immunoassay. Au/HGO was used as the substrate material of the immunosensor for capture of Ab_1.

Au/ZnO nanomaterial was synthesized to improve the sensitivity of the immunosensor by capturing the Ab_2/HRP. The dendritic shapes of ZnO had a large surface area to utilize the maximized Au particles, and abundant concurrent active sites on the surface were exposed to catalyse the reduction of H_2O_2. Hence, the detection signal of the immunosensor was amplified by the enhanced peroxidase-like properties. This work demonstrated the following advantages: the large surface area of the Au/HGO nanocomposite could remarkably increase the adsorption of Ab_1; and the peroxidase-like catalytic activity of Au/ZnO carrier could increase the load of the bioconjugate and simultaneously enhance the response signals of the immunosensor. The signal of the proposed immunosensor was linear from 0.001 to 100 ng·mL^{-1} CEA and had a low detection limit of 0.6 pg·mL^{-1} (S/N equals 3). The developed immunosensor was tested in CEA detection in human serum samples. The ultrasensitive immunosensor can be potentially used in clinical diagnostics.

2. MATERIALS AND METHODS

2.1. Materials and Equiment

Graphite powder was prepared in our laboratory. CEA and chloroauric acid ($HAuCl_4$) were purchased from Sangon Biotech (Shanghai, China). The mouse-derived McAb to CEA was purchased from Linc-Bio Science Co. Ltd (Shanghai, China). HRP-conjugated rabbit anti-mouse IgG was purchased from Sangon Biotech (Shanghai, China). $Zn(CH_3COO)\cdot 2H_2O$ was purchased from Tianjin Kermel Chemical Company (Tianjin, China). Bovine serum albumin (BSA) was obtained from Beijing Cell Chip Biotechnology Co., Ltd (Beijing, China).The chemicals and solvents used in the experiments were of analytical grade. Milli-Q water was used throughout the experiments. Phosphate buffer saline (PBS, pH 7.4) was acquired by mixing 0.01 M NaH_2PO_4 solution with 0.01 M Na_2HPO_4.

A JEOL 5160LV electron microscope was used for the acquisition of scanning electron microscopy (SEM) images. Transmission electron microscopy (TEM) images were obtained by a JEOL 2010 transmission electron microscope. A D8 ADVANCE X-ray diffractometer was used for X-ray diffraction (XRD) measurements.

2.2. Preparation of HGO

HGO was synthesized according to a previously reported procedure [20]. An aqueous solution of H_2O_2 (5 mL, 30% H_2O_2) and an aqueous dispersion of GO (50 mL, 2 mg/mL) were mixed and heated at 100 °C. The mixture was stirred for 120 min; the product was centrifuged, washed several times with pure water and re-dispersed in to a dark HGO solution (2 mg/mL) used in the experiments.

2.3. Preparation of Au/HGO Nanocomposite

The Au/HGO nanocomposite was synthesized by a single-step solve-thermal method [21, 22]. Initially, 60 mL of 0.5 mg/mL HGO solution was sonicated to obtain a homogeneous aqueous solution. Then, 1.69 mL of 10 mM $HAuCl_4$ solution was added to the HGO suspension. The mixture was

incubated at 0 °C under stirring for 30 min, centrifuged at 12,000 rpm for 30 min, and purified by washing 3-4 times with deionized water to obtain Au/HGO.

2.4. Preparation of ZnO Nanoparticles

ZnO nanoparticles were synthesized according to a previously reported simple solve-thermal procedure. Typically, 30 mL mixture of 1 mmol $Zn(CH_3COO)\cdot 2H_2O$ and 5 mmol NaOH was placed into a Teflon autoclave and incubated at 160 °C for 24 h. The products was centrifuged, washed 3-4 times with distilled water and absolute ethanol, and dried in a vacuum stove at 60 °C for at least 10 h [23].

2.5. Preparation of Au/ZnO Nanoparticles

The Au/ZnO nanoparticles were synthesized as follows: 0.11 mL of 0.24 M $HAuCl_4$ was added into 100 mL of 5 mmol/L ZnO solutions under stirring. After stirring at 110 °C for 15 min, 3 mL of 0.04 M $C_6H_5Na_3O_7$ was added to the reactants. After incubation for 40 min, the obtained pink product was centrifuged, washed several times with distilled water and absolute ethanol, and dried in a vacuum stove at 60 °C for half a day. The colour of the resulting product was changed from white to pink indicating that the AuNPs were successfully decorated on the ZnO microstructures to form Au/ZnO [23].

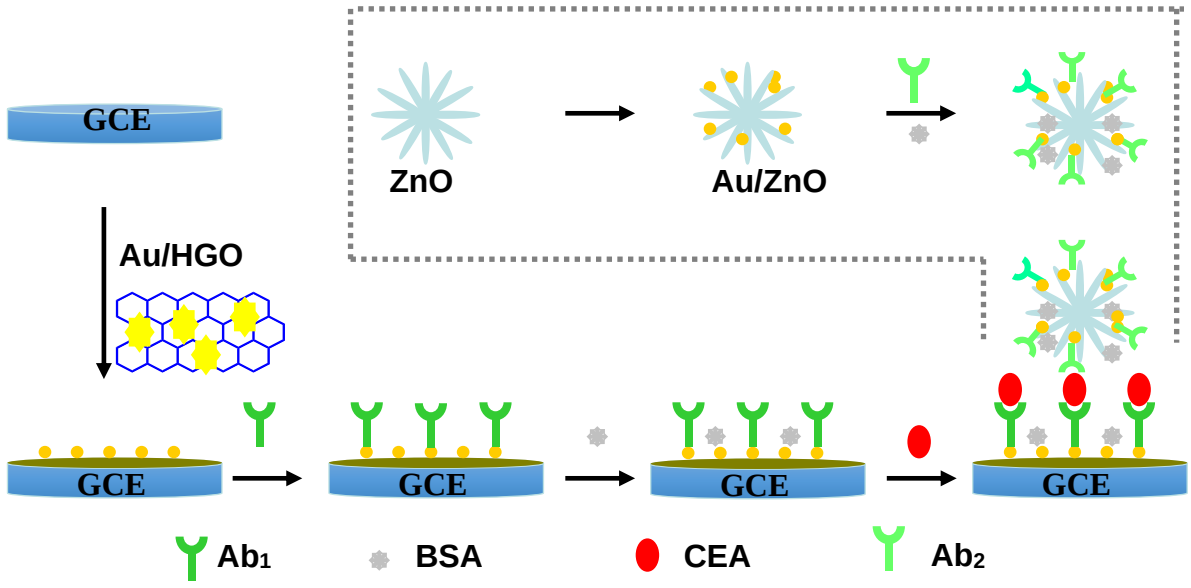

Scheme 1. The schematic illustration of the fabrication procedure of the CEA immunosensor

2.6. Preparation of Ab_2/HRP-Au/ZnO Bioconjugate

The solutions of Au/ZnO (2.0 mg/mL, 1 mL) and Ab_2 (10 μg/mL, 1 mL) were well mixed and stirred for 24 h at 4 °C. Then, 0.1% BSA was added to the mixture to block the remaining active sites on the surface of Au/ZnO. After centrifugation, the resulting Ab_2/HRP-Au/ZnO bioconjugate was dispersed in 1 mL PBS solution and stored in a 4 °C refrigerator.

2.7. Fabrication of the Electrochemical Immunosensor

Scheme 1 shows a schematic of fabrication process of the immunosensor. A glass carbon electrode (GCE) was mirror polished with 0.3 and 0.05 μm alumina slurry and cleaned by an ultrasonic cleaner with acetone, ethanol and pure water. The clear GCE was dried at room temperature before use; then, 15μL of the Au/HGO nanocomposite was dropped to cover the GCE surface; then 5μL of anti-CEA (60 μg/mL) was dropped evenly on the Au/HGO nanocomposites surface. The electrode was cleaned with pH 7.4 PBS and incubated in a refrigerator for half a day. Then, the Au/HGO/GCE was immersed in 1% BSA solution for half an hour at 37 °C to block the remaining active sites to avoid non-specific adsorption. Then, the immunosensor was cleaned with PBS and dried using a steam of high-purity nitrogen. Subsequently, the sensor was incubated in solutions with various concentrations of CEA for 40 min at 37 °C, washed with PBS solution and dried under a steam of nitrogen. Finally, the immunosensor was immersed in Ab_2/HRP-Au/ZnO solution prepared in Section 2.6 for sandwich immunoreaction. After cleaning with 0.01 M PBS, the immunosensor was dried using nitrogen gas.

2.8. Electrochemical Measurements

A Shanghai Chenhua CHI660E workstation was used to perform all electrochemical measurements. A conventional three-electrode system (a 3 mm diameter Au/HGO/GCE was used as a working electrode) was used for the measurements. Solutions were degassed with nitrogen to remove O_2. Cyclic voltammograms (CV) and electrochemical impedance spectroscopy (EIS) were performed in the electrolyte solution (10 mM PBS (pH 7.4) + 2 mM $[Fe(CN)_6]^{3-}$/$[Fe(CN)_6]^{4-}$ (1:1) + 0.1 M KCl). The differential pulse voltammetry (DPV) measurements were performed in 0.01M PBS (pH 7.4).

3. RESULTS AND DISCUSSION

3.1. Characterization of HGO, Au/HGO and Au/ZnO Composite

Figure 1A shows the morphology of the prepared HGO that had a disordered and folded multilayer surface, similar to layers of transparent tulle. Figure 1B shows the SEM image of the prepared Au/HGO. The bright spots in the SEM image correspond to the gold nanoparticles, with the sizes of approximately several tens of nanometres. Figure 1E shows the TEM image of the Au/HGO; the black dots correspond to the Au nanoparticles. The image indicates that the Au nanoparticles are clearly and homogeneously decorated on the graphene sheets [24]. Figures 1C, D demonstrate the

corresponding morphology of the synthesized ZnO and Au/ZnO. The ZnO product in Figure 1C includes of numerous needle-like microsized particles piled up into a sea-urchin-like shape. Additionally, the gold nanoparticles decorated on the surface can be detected in the Au/ZnO products in Figure 1D.

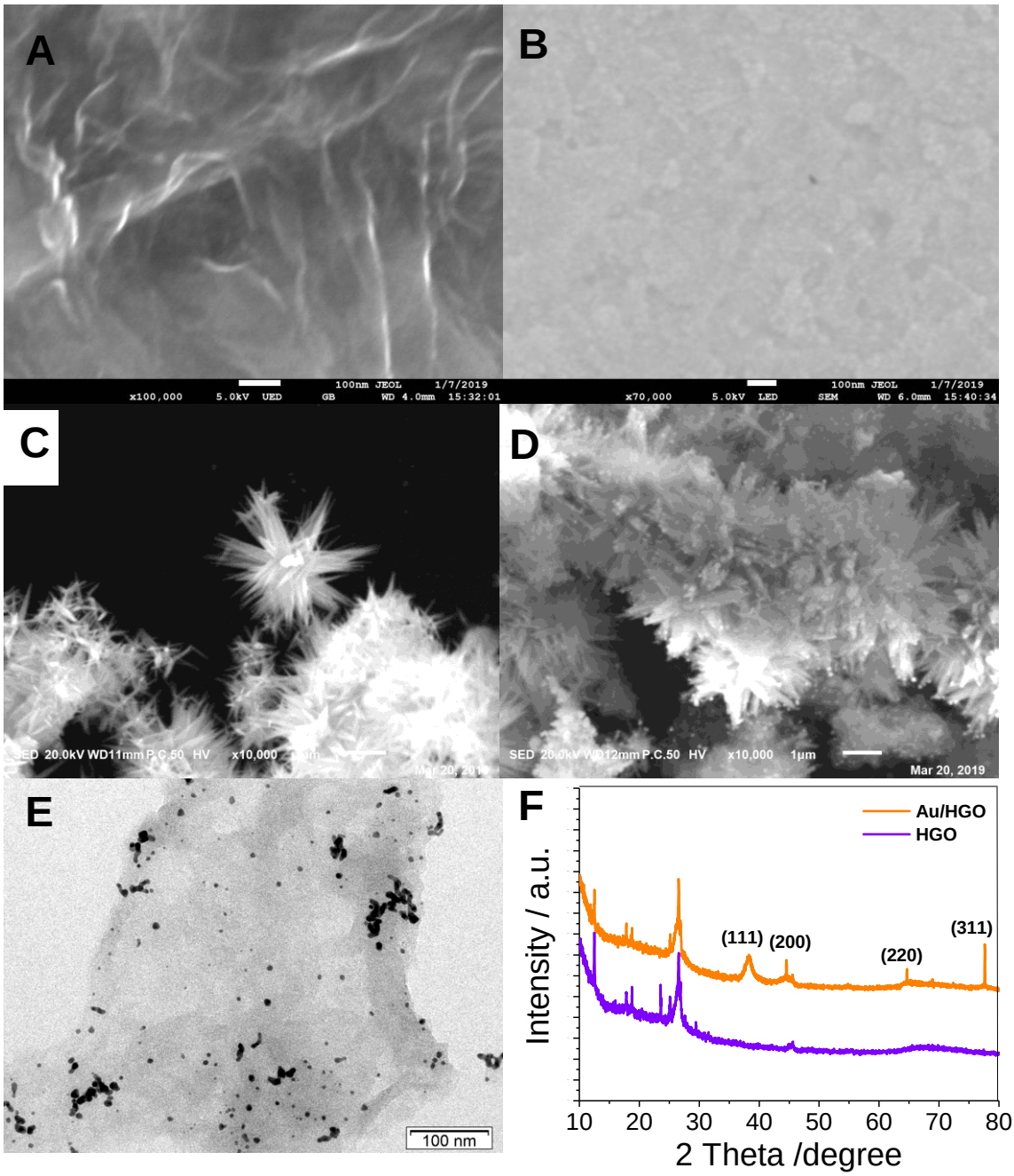

Figure 1. SEM images of (**A**) HGO; (**B**) Au/HGO; (**C**) ZnO; (**D**) Au/ZnO composites. (**E**) TEM of Au/HGO. (**F**) X-ray diffraction (XRD) patterns of Au/HGO and holey-graphene oxide (HGO).

The structural characteristics of the as-prepared Au/HGO composite structures were investigated by XRD as shown in Figure 1F. A broad peak observed at 26.8° implied that GO had been fully reduced, and the diffraction peak at 43° corresponded to the (100) plane of the hexagonal carbon

skeleton [25]. The XRD pattern of Au/HGO confirmed the fabrication of a face-centred cubic composition of Au nanoparticles. The diffraction peaks at 38.2°, 44.5°, 64.6° and 77.5° corresponded to (111), (200), (220) and (311) crystal faces of the Au nanoparticles, respectively. This result may indicate that the structure of the prepared Au/HGO composite includes gold nanoparticles apparently homogeneously dispersed on the outside of HGO, and that a part of Au nanoparticles could have aggregated on the surface of GO [25-27].

3.2. Electrochemical Characteristics of the Immunosensor

CV and EIS were used to study the modified process of the immunosensor. Figure 2A shows the CVs of $[Fe(CN)_6]^{3-}/[Fe(CN)_6]^{4-}$ in PBS using the bare (curve a), Au/HGO modified (curve b) and anti-CEA/Au/HGO (curve c) modified GCE. The changes in the amperometric response correspond to the obstruction of the electron transfer kinetics of the $Fe(CN)_6^{3-}/Fe(CN)_6^{4-}$ probe. An electrochemical signal was detected using bare GCE as shown in curve a. When the Au/HGO composite (curve b) was decorated on the GCE, a substantially higher peak was observed compared with that detected in the case of bare GCE, indicating that the Au/HGO composite markedly facilitated the electron transfer due to an increase in the electrode surface area and excellent conductivity. After Ab_1 was assembled on the surface of the Au/HGO electrode, the peak current of the redox couple was decreased accordingly, because the captured biomolecules, such as the antibodies, might form a blocking layer that can severely hinder the electron transfer between the probe and the electrode surface [28].

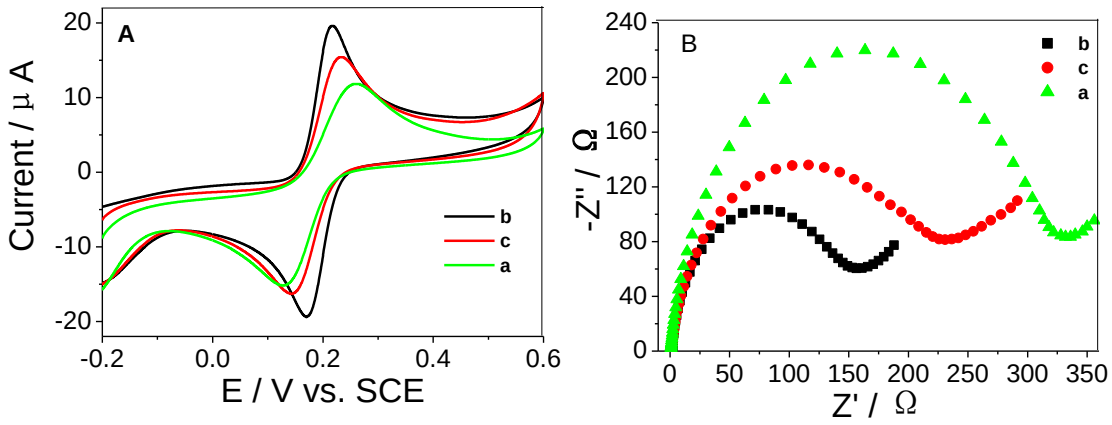

Figure 2. (**A**) CVs and (**B**) Nyquist plots of bare (**a**), Au/HGO modified (**b**), anti-CEA/Au/HGO modified (**c**), GCE in 0.10 M KCl containing 2×10^{-3}M $K_3[Fe(CN)_6]/K_4[Fe(CN)_6]$.

The EIS measurement was more sensitive in monitoring the changes in the interface features in the $[Fe(CN)_6]^{3-}/[Fe(CN)_6]^{4-}$ probes system of the modified electrodes. The impedance spectra included two parts: a semicircular fragment and a linear fragment. The former semicircle represents the electrochemical process of electron transfer process, and the latter represents the diffusion process [28-31]. The change of the resistance is associated with the diameter of semicircle fragment. Figure 2B shows the EIS of the electrode at various decorated states. For the bare GCE, a very small semicircle at high frequencies was observed with R_{et} (the electron transfer impedance) value of 320±10 Ω (curve a).

After Au/HGO was assembled on the electrode, the Au/HGO modified GCE showed a substantially lower resistance (curve b) with a decrease in the R_{et} value down to 140±5 Ω implying that the presence of Au/HGO increases the conductivity. Subsequently, when anti-CEA was immobilized onto the electrode, the R_{et} was increased to 220±5 Ω (curve c), which can be attributed to poor conductivity of the antibodies, thus, demonstrating the signal antibody was well immobilized on the electrode successfully.

3.3. Optimization of Synthesis Conditions of Nanocomposites and Immunoassay Conditions

To achieve the optimal performance of the immunoassay, the volume of Au/HGO, the amount of immobilized Ab_2/HRP and the incubation time were tested. As shown in Figure 3A, an increase in the volume of Au/HGO was associated with an increase in the current response of the immunosensor during the detection of CEA(4 ng mL^{-1}), indicating that higher load of Ab_1 on Au/HGO results in higher antigen binding. However, when the volume of Au/HGO was more than 15 μL, the peak currents were decreased due to an increase in the Au/HGO thickness, which has an adverse influence on the electron transfer. And GCE modified 15 μL Au/HGO has the highest electrocatalytic current peaks. Therefore, 15 μL Au/HGO was used for the preparation of the immunosensors.

In addition, effect of the concentration of Ab_2/HRP on the immunosensor has been examined. When the concentration of Ab_2/HRP was increased from 10 μg/mL to 60 μg/mL, the peak current was gradually increased and remained constant at Ab_2/HRP over 60 μg/mL (Figure 3B). This result indicates that when the concentration of Ab_2/HRP is under 60 μg/mL, there is not enough quantity Ab_2 to capture CEA; when the concentration of Ab_2/HRP is 60 μg/mL, Ab_2/HRP reaches the point of saturation on the surface of Au/ZnO, and the ability of capturing CEA reaches the best. Therefore, 5μL of 60 μg/mL of Ab_2/HRP was selected in the subsequent electrochemical experiments [32].

Figure 3C illustrates the relationship between the incubation time and the analytical performance of the immunoassay. Longer incubation time corresponds to higher DPV responses for CEA. After 40 min, the DPV current tends to stay constant, indicating that, CEA antigen adsorption by the capture antibody reached saturation, and that the binding of the capture antibody to Ab_2/HRP-Au/ZnO on the electrode surface also reached saturation, Therefore, 40 min incubation time was selected for the subsequent experiments [15, 33].

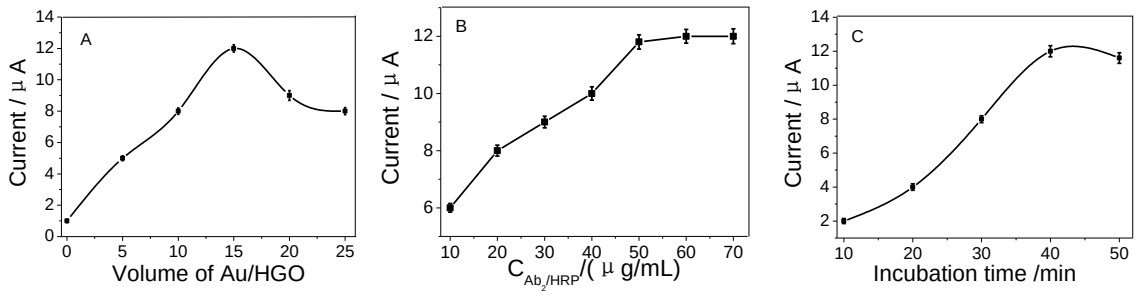

Figure 3. Effect of (**A**) the volume of Au/HGO, (**B**) the Ab_2 concentration and (**C**) the incubation time on the DPV response during the detection of CEA.

3.4. Quantitative Detection of CEA

DPV has higher sensitivity than CV and, hence, is usually used for quantitative detection in electrochemistry. The prepared sandwich-type electrochemical immunosensor was used to detect various concentrations of CEA by DPV in 0.01 M PBS (pH 7.4) from 0.1 to - 0.6 V. The results of the DPV analytical performance of the CEA immunosensor are shown in Figure 4.

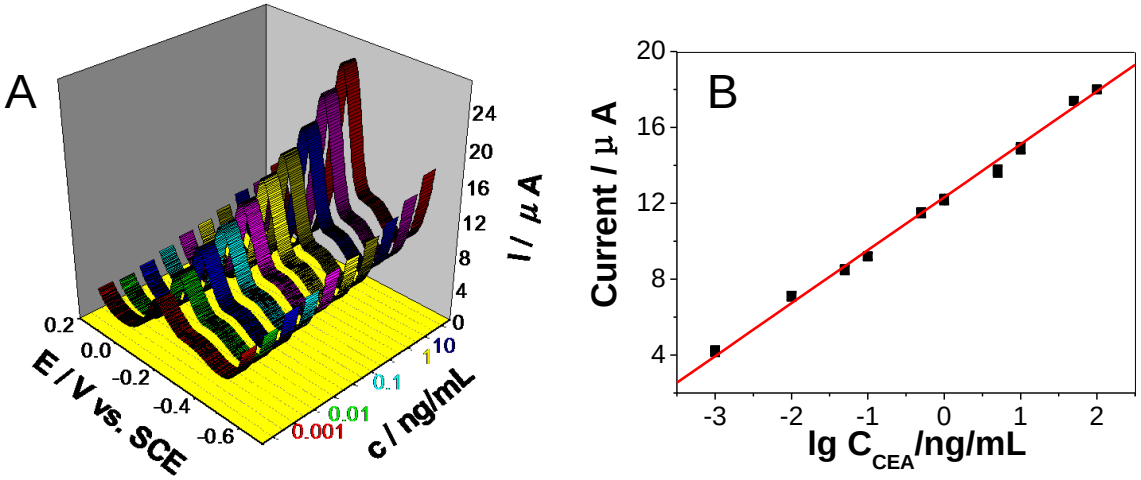

Figure 4. (**A**) DPV responses of the proposed immunosensor after incubation with various concentrations of CEA in 0.01 M PBS (pH 7.4) (0.001, 0.01, 0.05, 0.1, 0.5, 1, 5, 10, 50 and 100 ng·mL^{-1}). (**B**) Linear relationship between the current I of the immunosensor and logarithm of CEA concentration. Error bars represent the standard deviation, n=5.

Table 1. Comparison of the characteristics of various modified electrodes.

Electrode	Detection range (ng mL^{-1})	Detection limit (ng mL^{-1})	Method	Refs.
NH_2-G/THi/AuNPs	0.05 - 500	0.01	DPV	[34]
AuNP/IL/PICA/erGO	0.02 - 90	0.02	DPV	[35]
Au/ZnO NPs	0.1 - 70 - 200	0.01	FFTCCV	[36]
AuNPs/PDDA/rGO-$BaYF_5$	0.001 - 80	0.0087	ECL	[37]
IL-rGO-AuNPs	0.01 - 100	0.01	DPV	[38]
Au/ZnO and Au/HGO	0.001 - 100	0.0006	DPV	this work

The data of Figure 4A indicate that the current response of the DPV signal intensity of the CEA detection is gradually increased concomitant to an increase in the concentration of CEA. From the former to the latter along the Y axis, these curves represent the electrocatalytic current responses of the immunosensor of CEA detection: 0.001, 0.01, 0.05, 0.1, 0.5, 1, 5, 10, 50 and 100 ng·mL^{-1} ng/mL. An increase in the peak current value was proportional to the logarithmic values of the concentration of

CEA within the linear range from 0.001 ng mL^{-1} to 100 ng mL^{-1}. The linear regression equation of the calibration curve was I=12.32+2.793 log C_{CEA} (ng mL^{-1}) with the correlation coefficient of 0.9980. A detection limit of 0.6 pg·mL^{-1} (S/N=3) was observed. Compared to other methods previously reported in the literature for quantitative detection of CEA, the results obtained using our immunosensor indicate a prominent liner range and a superior sensitivity (Table 1). The results might be primarily attributed to the following factors: First, Au/HGO has high electronic conductivity, strong adsorption and large surface area that ensures successful conjugation of Ab_1 to sensitively monitor trace amounts of CEA. Second, Au@ZnO with more active sites could increase electrocatalytic response to the reduction of H_2O_2. Third, the peroxidase-like catalytic activity of Au/ZnO and Ab_2/HRP-Au/ZnO has a high affinity interconnected with CEA that can strengthen the sensitivity of the immunosensor [4, 32, 39].

3.5. Specificity, Reproducibility, and Stability of the Immunosensor

Specificity is a very important parameter for the application of the developed immunosensor in the analysis of biological samples. To confirm the selectivity of the proposed immunosensor to CEA, possible interference was determined by the same approach used in the case of CEA analysis; the test samples contained prostate-specific antigen (PSA), human IgG, BSA, UA, glucose, hepatitis B surface antigen (HBs) and L-Tyr. The results of Figure 5 show that less than 5% of the current variation was influencd by the addition of the interfering substances. The concentration of CEA was 1 ng·mL^{-1} while the concentrations of the other interferences were 50 ng·mL^{-1}. The data indicate an acceptable precision of the developed immunosensor.

The reproducibility of the designed CEA immunosensor was investigated by assessing five parallel samples containing 1.0 and 10.0 pg·mL^{-1} CEA solutions. The relative standard deviation of the five measurements was 4.32% and 5.18%, respectively, indicating that the proposed immunosensor has satisfactory reproducibility and gratifying precision.

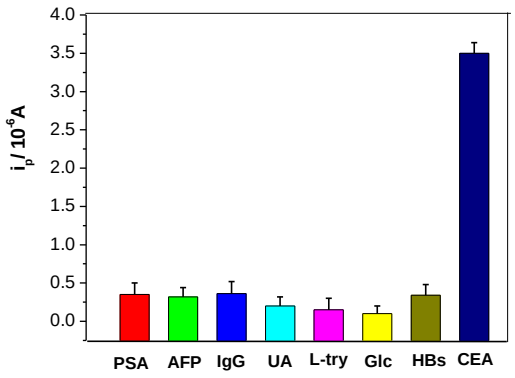

Figure 5. Study of the specificity of the immunosensor towards various interferences; concentrations of PSA, human IgG, BSA, UA, Glc (glucose), L-Tyr and HBs were 10 ng·mL^{-1}. The concentration of CEA was 1 ng·mL^{-1}. Error bars represent the standard deviation, n=5.

The stability of the immunosensor was evaluated by detecting the changes in the DPV signals after the sensor was not used for a period of time. After storage at 4 °C for 7 days, the immunosensor retained 95.2% of its initial current peaks, indicating that the developed CEA immunosensor had an acceptable stability. Therefore, the developed immunosensor can be used for quantitative detection of CEA with high sensitivity, acceptable stability and reproducibility.

3.6. Real sample analysis

Based on the above research, the proposed immunosensor could be used to detect the content of CEA in the serum. To demonstrate the feasibility of the application of the immunosensor, various concentrations of CEA were added into human serum samples using a standard addition method. The experimental results detected are exhibited in Table 2. The recoveries ranged from 97% to 105.05% and the RSD ranged from 4.54% to 1.93%, indicating that the developed immunosensor could achieve high accuracy for the detection of CEA in the human serum for clinical diagnosis.

Table 2. The results of CEA detection in the human serum samples.

Samples	Added (ng mL^{-1})	Found (ng mL^{-1})	Recovery (%)	RSD (%)
1	0.01	0.0097	97.00	3.97
2	1.00	0.99	99.00	4.54
3	5.00	5.22	104.40	3.02
4	10.00	10.12	101.20	3.25
5	20.00	21.01	105.05	2.04
6	30.00	29.92	99.73	1.93
7	50.00	49.23	98.46	2.91

4. CONCLUSIONS

In summary, a convenient and sensitive sandwich-type electrochemical immunoassay for the ultra-quantitative detection of CEA was developed by using Au nanopaticles/holey graphene oxide and Au/ZnO composites. Au/HGO with large surface area and excellent conductivity was used as the substrate material of the immunosensor to capture Ab_1. An Au/ZnO nanomaterial with peroxidase-like catalytic activity was used to capture Ab_2/HRP. Under the optimal conditions, a linear range of 0.001 - 100 ng·mL^{-1} CEA and a low detection limit of 0.6 pg·mL^{-1} CEA (S/N=3) were observed. The developed immunosensor was applied to detect CEA in human serum samples. The proposed electrochemical immunoassay has high selectivity, satisfactory reproducibility and long-term stability, thus suggesting promising application prospects in disease diagnostics and clinical analysis.

ACKNOWLEDGEMENTS
This work was financially supported by projects of the National Natural Science Foundation of China (U1404824, 81741147), Henan International Cooperation in Science and Technology (172102410083), the Natural Science Foundation of the Henan Province (182300410270) and Technicians Troop Construction Projects of Henan Province.

References

1. A. Jemal, R. Siegel, J.Q. Xu, E. Ward, *Ca-a Cancer Journal for Clinicians*, 60 (2010) 277.
2. G. Liang, S. Kan, Y. Zhu, S. Feng, W. Feng, S. Gao, *International Journal of Nanomedicine*, 13 (2018) 585.
3. E. Xiong, L. Jiang, *Analyst*, 144 (2019) 634.
4. F. Pei, P. Wang, E. Ma, H. Yu, C. Gao, H. Yin, Y. Li, Q. Liu, Y. Dong, *Biosens. Bioelectron.*, 122 (2018) 231.
5. Y. Tsutsumi, H. Nagura, K. Watanabe, *American journal of clinical pathology*, 82 (1984) 535.
6. K. Kubota, H. Nakanishi, N. Hiki, N. Shimizu, E. Tsuji, H. Yamaguchi, K.-I. Mafune, T. Tange, M. Tatematsu, M. Kaminishi, *International journal of cancer*, 105 (2003) 136.
7. Y.S. Liu, W. Wang, W.H. Hu, Z.S. Lu, X.Q. Zhou, C.M. Li, *Biomed. Microdevices*, 13 (2011) 769.
8. C.L. Ren, P. He, J.Q. Zhang, Z.X. Zheng, Y.Y. Qiao, X.H. Zhao, *Cancer Biol. Ther.*, 11 (2011) 633.
9. X.M. Ma, Y. Lin, L.H. Guo, B. Qiu, G.N. Chen, H.H. Yang, Z.Y. Lin, *Biosens. Bioelectron.*, 87 (2017) 122.
10. L. Chen, X. Zeng, P. Si, Y. Chen, Y. Chi, D.-H. Kim, G. Chen, *Analytical Chemistry*, 86 (2014) 4188.
11. W.T. Shi, Z.F. Ma, *Biosens. Bioelectron.*, 26 (2011) 3068.
12. J.N. Tian, L.J. Zhou, Y.C. Zhao, Y. Wang, Y. Peng, S.L. Zhao, *Talanta*, 92 (2012) 72.
13. T.-W. Chen, X.-N. Yu, S.-J. Liz, *International Journal of Electrochemical Science*, 14 (2019) 7037.
14. Y. Xu, C.Y. Chen, Z. Zhao, Z. Lin, C. Lee, X. Xu, C. Wang, Y. Huang, M.I. Shakir, X. Duan, *Nano Letters*, 15 (2015) 4605.
15. S. Akbari Nakhjavani, H. Afsharan, B. Khalilzadeh, M.H. Ghahremani, S. Carrara, Y. Omidi, *Biosens. Bioelectron.*, 141 (2019) 111439.
16. F. Schuett, V. Postica, R. Adelung, O. Lupan, *Acs Applied Materials & Interfaces*, 9 (2017) 23107.
17. Y. Zhang, S. Zhang, M. Zheng, H. Pang, *International Journal of Electrochemical Science*, 10 (2015) 8706.
18. Z. Yanguang, F. Xiaofei, G. Yousong, Y. Xiaoqin, K. Zhuo, Z. Xin, L. Pei, Z. Leichao, Z. Yue, *Colloids & Surfaces B Biointerfaces*, 126 (2015) 476.
19. W. Yinyin, L. Ying, L. Xiaoqian, X. Yuezhong, S. Guoyue, J. Litong, *Biosens. Bioelectron.*, 26 (2011) 275.
20. H. Sun, L. Mei, J. Liang, Z. Zhao, C. Lee, H. Fei, M. Ding, J. Lau, M. Li, C. Wang, *Science*, 356 (2017) 599.
21. F. Xian, J. Liu, W. Jing, Z. Hong, H. Ren, Z. Li, *Biosens. Bioelectron.*, 97 (2017) 218.
22. A.H. Jing, G.F. Liang, Y.X. Yuan, W.P. Feng, *Micromachines*, 10 (2019) 84.
23. W. Xia, C. Mei, X. Zeng, G. Fan, J. Lu, X. Meng, X. Shen, *Acs Applied Materials & Interfaces*, 7 (2015) 11824.
24. G. Darabdhara, M.R. Das, S.P. Singh, A.K. Rengan, S. Szunerits, R. Boukherroub, *Advances in colloid and interface science*, 271 (2019) 101991.
25. M.-Q. Yang, X. Pan, N. Zhang, Y.-J. Xu, *Crystengcomm*, 15 (2013) 6819.
26. M. Tang, X. Wang, F. Wu, Y. Liu, S. Zhang, X. Pang, X. Li, H. Qiu, *Carbon*, 71 (2014) 238.
27. T. Wei, J. Sun, F. Zhang, J. Zhang, J. Chen, H. Li, X.-M. Zhang, *Catalysis Communications*, 93 (2017) 43.
28. G. Yang, J. Cao, L. Li, R.K. Rana, J.J. Zhu, *Carbon*, 51 (2013) 124.
29. I. Navratilova, P. Skladal, *Bioelectrochemistry (Amsterdam, Netherlands)*, 62 (2004) 11.
30. Y. Li, Y. Chen, D. Deng, L. Luo, H. He, Z. Wang, *Sensors and Actuators B-Chemical*, 248 (2017) 966.
31. C. Zhang, S. Zhang, Y. Jia, Y. Li, P. Wang, Q. Liu, Z. Xu, X. Li, Y. Dong, *Biosens. Bioelectron.*, 126 (2019) 785.

32. L. Tian, L. Liu, Y. Li, Q. Wei, W. Cao, *Scientific Reports*, 6 (2016) 30849.
33. Z. Cui, D. Wu, Y. Zhang, H. Ma, H. Li, B. Du, Q. Wei, H. Ju, *Anal. Chim. Acta*, 807 (2014) 44.
34. Y. Wang, H. Xu, J. Luo, J. Liu, L. Wang, Y. Fan, S. Yan, Y. Yang, X. Cai, *Biosens. Bioelectron*., 83 (2016) 319.
35. D. Zhao, Y. Wang, G. Nie, *Microchimica Acta*, 183 (2016) 2925.
36. P. Norouzi, V.K. Gupta, F. Faridbod, M. Pirali-Hamedani, B. Larijani, M.R. Ganjali, *Analytical Chemistry*, 83 (2011) 1564.
37. L. Zhao, J. Li, Y. Liu, Y. Wei, J. Zhang, J. Zhang, Q. Xia, Q. Zhang, W. Zhao, X. Chen, S*ensors and Actuators B-Chemical*, 232 (2016) 484.
38. N. Liu, Z. Ma, *Biosens. Bioelectron*., 51 (2014) 184.
39. H. Lv, Y. Li, X. Zhang, Z. Gao, C. Zhang, S. Zhang, Y. Dong, *Biosens. Bioelectron*., (2018) 1.